JOURNAL OF PROPULSION AND POWER
Vol. 11, No. 6, November–December 1995

Studies of Helical Magnetohydrodynamic Seawater Flow in Fields up to Twelve Teslas

T. F. Lin* and J. B. Gilbert†
Pennsylvania State University, University Park, Pennsylvania 16802

This article discusses analytical and experimental studies of a helical magnetohydrodynamic (MHD) seawater thruster (or pump) device using a 12-T superconducting solenoid magnet. This magnet is situated and the experiments are conducted at Francis Bitter National Magnet Laboratory of the Massachusetts Institute of Technology. Analytical models are developed to predict the performance of the helical MHD thruster in a closed-loop environment. The analytical results are compared with experimental data and good agreement is obtained. A significant increase in MHD energy conversion efficiency compared to the same thruster at lower magnetic field strengths (6–8 T) is realized. A significant increase in the maximum fluid velocity, from 2.5 m/s at the 8-T electromagnet, to 3.7 m/s, is also realized. For the first time in our experimental MHD thruster studies, a gross mechanical efficiency greater than 10% is observed.

I. Introduction

THE presence of salts allows seawater to conduct electricity by electrolytic ion exchange. Thus, by passing an electric current through seawater in the presence of a magnetic field, a Lorentz ($J \times B$) force will act to move the seawater in a direction normal to a plane containing both the magnetic field and electric current vectors. This is the basis for seawater magnetohydrodynamic (MHD) propulsion for marine vehicles. Few mechanical moving parts are required with MHD propulsion. As a result, this type of propulsion may be very quiet. Although it is not clear that MHD propulsion will be more efficient than the conventional systems using propellers, its potential acoustic quietness is of interest to the U.S. Navy from a strategic point of view. Nevertheless, one must note that while it may eliminate the noise from rotating machinery and propellers, the noise created by bubbles at the electrodes must be ascertained before its acoustic advantages can be confirmed.

MHD propulsion receives more serious attention with the advent of multi-Tesla superconducting magnets. With superconducting magnets, the magnetic field strength is increased and the magnet's weight and electrical consumption are decreased significantly. Weight is, however, still a major concern in MHD propulsion, even for superconducting magnets, because massive structural enforcement materials are required to maintain the magnet integrity at high fields. In general, on the basis of the same warm bore volume, a superconducting solenoid (for helical thruster) requires significantly less structural materials and weight than a dipole (for linear thruster) due to its symmetrical coil winding. Additionally, significantly higher magnetic fields are attainable by solenoid magnets, and therefore, by helical thrusters.

Recently, there has been an increase of research and development in this field, as summarized by Lin.[1] An experimental ship, Yamato-1, utilizing MHD propulsion has recently been built and tested in Japan.[2] Research in the U.S. includes laboratory closed-loop experiments at the Argonne National Laboratory (ANL),[3] Naval Undersea Warfare Center–Newport (NUWC–N),[4] and Applied Research Laboratory of Pennsylvania State University (ARL–Penn State).[5] Analytical studies of seawater MHD propulsion,[6,7] and seawater electrolysis, conductivity enhancements, and electrode studies[8,9] have also been conducted. The experiments of ANL, NUWC–N, and ARL–Penn State use 6-, 3.2-, and 8-T magnets, respectively. Among them, the magnets for ANL and NUWC–N are superconducting dipoles, while the one for ARL–Penn State is an electrosolenoid. The analytical studies have not considered the effects of electrolytic bubbles on the performance of MHD thrusters. Subsequent studies by Lin et al.[10] have included these effects. During the electrolysis of seawater, $H_2(g)$ is produced at the cathode while a $Cl_2(g)/O_2(g)$ mixture is produced at the anode. The distribution of $Cl_2(g)$ and $O_2(g)$ is determined from the electrode materials used. For a given current, the volumetric production rates of both the $H_2(g)$ and $Cl_2(g)/O_2(g)$ mixtures can be determined since they are linearly proportional to the applied current. A significant portion of anode gases, Cl_2 and O_2, subsequently dissolves back to seawater. As a result, the void fraction of electrolytic gases for the experiments in this work is generally less than 1%. Therefore, the two-phase effects have not been significant.

The aforementioned studies have concentrated on linear MHD channels as illustrated by Fig. 1. These systems, with the exception of Ref. 5, utilize the long-bore and lower-magnetic-field dipoles (≤6 T). Unfortunately, a dipole magnet requires an extensive structural support that limits its attainable magnetic field. Much higher fields can presently be achieved with large diameter bore solenoid magnets due to their symmetric coil windings. However, straight MHD thrusters when used in solenoid magnets have limited thrust due to small aspect ratios (ARs).[5]

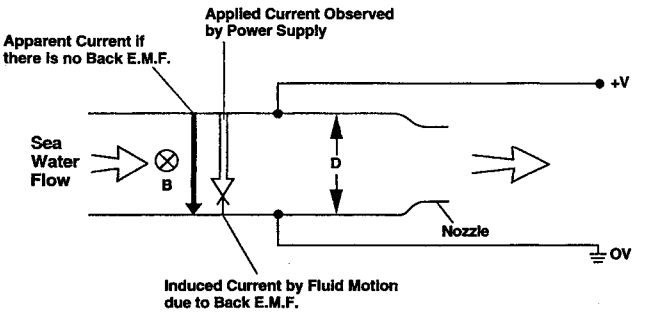

Fig. 1 Illustration of the linear duct MHD channel.

Received Jan. 26, 1994; revision received Nov. 25, 1994; accepted for publication Jan. 5, 1995.

*Senior Research Associate, Applied Research Laboratory. Member AIAA.

†Research Assistant, Applied Research Laboratory.

Taking advantage of the high-field characteristics of a solenoid, single- and double-loop cyclotron-type systems has been investigated by Lin et al.[11] In the cyclotron design, the magnetic field and electric current are applied axially and radially, respectively. As a result, the MHD flow is induced in the azimuthal direction allowing for an increased active length and the utilization of higher magnetic field near the winding. Results from these studies are very encouraging with the two-loop system, exhibiting a higher efficiency than the single-loop system. A logical evolution from this approach is the utilization of the entire length of the solenoid bore via a helical flow passage. Results of this type of helical thruster in a magnetic field range from 6 to 8 T have been reported.[12] These results suggest the helical thruster can achieve high velocity with reasonable flow rate, mainly due to the increased thruster aspect ratio (L/D) and high magnetic field. With high magnetic field and high flow velocity, the helical thruster also demonstrates a higher efficiency than earlier linear versions.

This article reports results of the same helical thruster using an even higher field (12-T) superconducting solenoid magnet at MIT's Francis Bitter National Magnet Laboratory (FBNML). The performance characteristics (flow rate, thrust, and mechanical efficiencies) of the thruster are measured and compared with theoretical predictions. The fluid used is a commercially available substitute for seawater that meets ASTM standard D1141-52. For simplicity, this sea–salt solution will be referred to as seawater in the remainder of this article.

II. Analytical Models

For the analyses that follow to be valid, MHD approximations of the seawater flows are assumed. They are supported by the fact that, for the flow of interest, the Maxwell's and fluid equations take the nonrelativistic form and only the induced electric field is significant. The induced magnetic field is negligible. While the range of magnetic field in this study is the highest among all seawater MHD facilities surveyed, due to the low conductivity of seawater [$\approx 4.5\ (\Omega m)^{-1}$], a typical value of the interaction parameter, N_1 = (Lorentz force)/(inertial force), is only estimated to be about 0.01.

To predict the performance of the helical thruster in a closed-loop, analytical models are developed. They calculate the MHD-induced flow rate by equating the pressure rise in the thruster to the sum of all hydraulic losses around the loop. In order to simplify calculation and more accurately model the system, the MHD pumping region is divided into a variable number of segments where certain parameters vary as functions of location, as discussed next.

A. Pressure Rise in the MHD Pumping Region

Figure 2 shows the helical MHD thruster at the left with its outer Hastelloy-C electrode at the right. Details of this helical test section are discussed in Sec. III.B. According to the Lorentz law, the force created by the thruster is

$$\boldsymbol{F} = \boldsymbol{J} \times \boldsymbol{B} \tag{1}$$

where $\boldsymbol{F}$ is the resultant Lorentz force vector, $\boldsymbol{J}$ is the electric current density vector, and $\boldsymbol{B}$ is the magnetic flux density vector. Due to the fact that the magnetic field strength and electric current (or current density) are functions of position in the magnet, the pressure rise is calculated for each segment in the MHD pumping region. Therefore, the total pressure rise due to the MHD effect in the direction of flow is given by

$$\Delta p_{\mathrm{MHD}} = \frac{\cos\theta}{A_{\mathrm{flow}}} \sum_{j=1}^{N} I_j B_j D \tag{2}$$

where j is the segment index, N is the total number of segments, I_j is the current in segment j, B_j is the axial magnetic field in segment j, D is the gap distance between electrodes, A_{flow} is the cross-sectional area of the helical flow channel; and θ is the rise angle of the centerline of the flow passage. For the 12-T superconducting magnet used, the axial component of the magnetic field vector as a spatial function in the magnet bore yields B_j. In the helical thruster, the electric current density decreases from the inner to outer electrode at a rate of $1/r$. Meanwhile, B_j increases from the inner to outer electrode allowing the radial reduction of MHD pumping to be compensated. Although the flow in the thruster is expected to be multidimensional, quasi-one-dimensional flow is presently treated for analytical simplicity. Current, instead of current density, in each flow segment is computed based on the applied voltage. Axial variation of B_j, at an averaged radial location between the inner and outer electrodes, has also been considered.

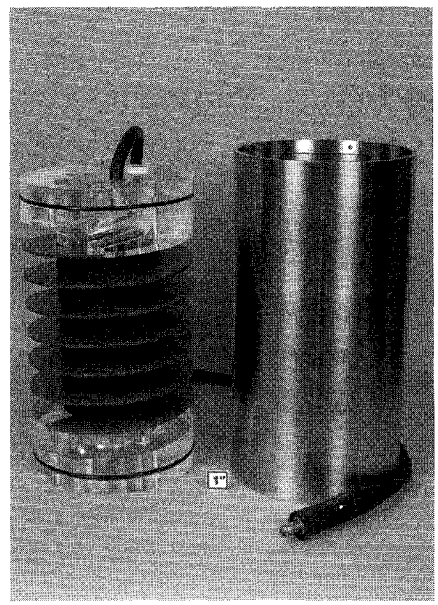

Fig. 2 Internal assembly and outer shell of the helical thruster.

B. Relationship Between Voltage and Current

In order to use Eq. (2), the relationship between the current, magnetic field, fluid velocity in the test section U and overpotential V_0 (the minimum voltage required to start a current) must be ascertained for each segment. There are two phenomena that diminish the useful electric potential: the back electromotive force (EMF) and the overpotential. The magnitude of the back EMF is given by

$$V_B = BUD \tag{3}$$

In contrast to experiments discussed in Ref. 12, the polarities of electrodes in the current experiments have been reversed due to the up-field orientation of the superconducting magnet. With this setup, the dimensional stable electrode (DSE) is actually a cathode, while the Hastelloy-C shell becomes an anode. The overpotential for this electrode arrangement is experimentally determined to be approximately 2.41 V. Therefore, the current in segment j can be calculated from

$$I_j = \frac{V - V_0 - B_j U_j D}{R_j} \tag{4}$$

where R_j is the resistance of segment j, and U_j is the fluid velocity in segment j. To calculate the resistance of each segment in the test section the following equation is employed:

$$R_j = \frac{\ell n(r_o/r_i)}{\phi_j w \sigma_{\mathrm{eff}}} \cos\theta \tag{5}$$

where r_o is the radius of outer anode, r_i is the radius of inner cathode, ϕ_j is the angle subtended by segment j, w is the height of flow passage or pitch of the helical fins, and σ_{eff} is the effective specific conductivity of seawater.

The specific conductivity of seawater at room temperature is between 4–5 $(\Omega\text{m})^{-1}$. However, as the experiment progresses, the temperature and chemical composition of water will change. Both of these effects will have a significant impact on the conductivity of seawater. Therefore, the effective conductivity is experimentally determined for each set of experiments from the voltage–current relationship.

C. Calculation of Pressure Drop

The previous equations can be used to calculate the MHD-induced gross pressure rise in the thruster, which in steady-state operation is equal to the sum of all frictional and form losses in the test loop. Although two-phase effects are not significant, the loop is still divided into two parts, a single-phase region and a two-phase region. As seen in Fig. 3, the single-phase region extends from the outlet of the tank to the entrance of the test section. The two-phase region is created by electrolytic bubbles at the electrodes and extends from the entrance of the test section to the inlet of the tank. Also, since the loop is modeled as a closed system, all gravitational terms are omitted because the two-phase density changes are negligible. This is especially true when the void fraction in the loop is small.

In each region, there are both frictional and form losses. In order to model the form losses, equivalent numbers of nominal pipe diameters are determined for the 90-deg elbows, tees, and valves.[13] Detailed discussion of the expansion and contraction losses in the loop is covered by Gilbert et al.[12] The pressure drop associated with the azimuthally turning fluid in the helical passage of the test section is also handled with a form factor given by[13]

$$K_b = (n - 1)\left(\frac{\pi}{4} f \frac{r}{D_h} + \frac{K}{2}\right) + K \tag{6}$$

where n is the number of 90-deg turns, D_h is the hydraulic diameter of the helical flow channel, r is the radius of curvature of the 90-deg turn, f is the friction factor, and K is the form factor of a single 90-deg turn.

K in Eq. (6) is given as a multiple of f and varies as a function of r/D_h. Therefore, this turning form factor can be expressed as an equivalent number of hydraulic diameters of a straight channel. However, due to the unique helical flow passage, the value of K is parametrically varied to best match the experimentally calibrated pressure drop data of the test section. A K value of approximately $8f$ is currently used. Since the path traversed by fluid is helical, the actual length L of the passage is given by $L_c/\cos\theta$, where L_c is $\pi(r_o + r_i)$, multiplied by the total number of revolutions in the helix. The form loss associated with the flow meter is determined from a correlation provided by the vendor. Frictional losses for straight pipe sections are handled using the standard method of calculating a friction factor for a pipe flow. The Darcy–Weisbach friction factor f is obtained from Incropera and Dewitt.[14]

Since viscosity affects the calculation of Reynolds number, which is used to obtain f, changes of viscosity due to the change of fluid temperature must be considered. Because of the Joule heating of seawater, as observed from the experiments, correlations from Whitfield and Jagner[15] based on seawater at a 35% salinity to account for the viscosity change are used.

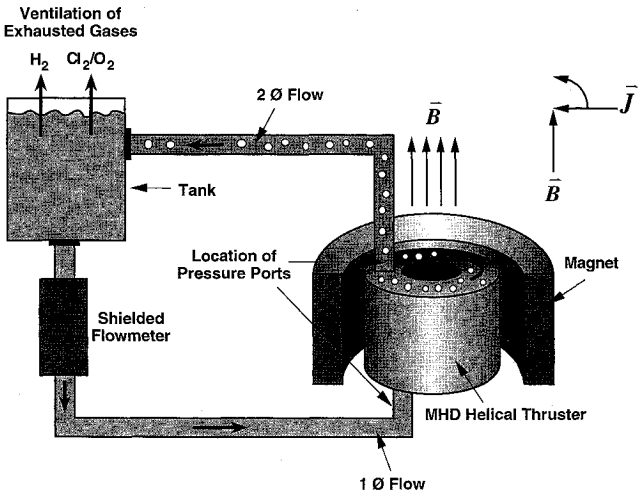

Fig. 3 Schematic of the helical thruster, 12-T superconducting magnet, and the loop (not drawn to scale).

D. Determination of Thrust and Efficiency

Once the MHD pressure rise is known, the gross thrust and efficiency can be calculated. From Eq. (2), the gross thrust produced by the thruster is given by

$$T = \Delta p_{\text{MHD}} A_{\text{flow}} \tag{7}$$

This gross thrust includes pressure losses within the thruster. Therefore, a more useful thrust, net thrust, is defined as the thrust due to the net pressure rise of the MHD thruster. The pressure rise across the thruster Δp_{net} is experimentally measured and is a net result of the MHD pressure rise minus the internal losses of the thruster. The net thrust is

$$T_{\text{net}} = \Delta p_{\text{net}} A_{\text{flow}} \tag{8}$$

The gross mechanical efficiency is a measure of how well the thruster converts electrical power into mechanical power and is defined as

$$\eta_m = \frac{\text{mechanical power produced}}{\text{electrical power consumed}} = \frac{TU}{VI} \tag{9}$$

The velocity in Eq. (9) is the fluid velocity in the test section. For the same reason discussed in Eqs. (7) and (8), there will be a gross mechanical efficiency η_m based on T, and a net mechanical efficiency $\eta_{m,\text{net}}$ based on T_{net}.

In the development of the computer code, Eq. (9) is used to determine the mechanical efficiency of the MHD thruster.

E. Solution Technique

The previous equations are incorporated into a computer code that predicts the performance characteristics of a helical thruster in a test loop. An iterative process is used to calculate the correct mass flow rate, for a given voltage. The code uses the magnetic field strength at the center of the bore and the voltage across the test section as inputs. The spatial distribution of axial magnetic field would linearly vary with the input field at the center of bore. First, a reasonable estimation of fluid velocity in the thruster is made. From the current [Eq. (4)] the pressure rise and segment pressure drop are determined. The test section pressure drop terms are added to the pressure drop in the remainder of the loop. If the total pressure drop around the loop is smaller than the pressure rise in the thruster, a larger mass flow rate is used in the next iteration. If the thruster pressure rise is smaller in magnitude, a lower mass flow rate is used as the next guess. This process continues until the following criterion is met:

$$\frac{|\Delta p_{\text{MHD}} - \Delta p_{\text{loop}}|}{\Delta p_{\text{MHD}}} \leq \times\ 10^{-6} \tag{10}$$

where Δp_{loop} is the total pressure drop of the loop including the test section.

The code just described can be used with different magnetic field strengths and electric potentials as inputs. These different conditions allow the theoretical effects of the two parameters to be examined. As depicted by Fig. 2, the inner electrode (DSE) only makes contact with fluid for six helical revolutions. On the other hand, the outer electrode (Hastelloy-C) makes at least partial contact with fluid for one additional revolution, half at the upstream and half at the downstream acrylic sections. The computer code simulates the test section as if the conducting region includes all seven loops, assuming the electric fringe effect occurs. The six-conducting-loop and six and one-half-conducting-loop models have also been simulated, but the seven-loop model agrees better with the experimental data. It is concluded that the fringe field at the ends of the inner electrode contributes to a significant MHD pumping, as if the seventh loop is active.

III. Experimental Apparatus

A. Seawater Loop

As shown in Fig. 3, the closed seawater loop is installed in and around the magnet. The loop has a 0.44-m^3 tank (upper left) that contains a premixed sea–salt solution. Once the MHD pumping commences, seawater is drawn from the bottom of the tank where a portion is diverted through a conductivity probe. The entire flow then passes through a turbine flow meter and enters the test section inside the magnet. The flow in and beyond the test section becomes two-phase as a result of electrolysis. Because the bubbles tend to float up due to buoyancy effect, the plumbing downstream of the test section is designed to run vertically upward to ensure removal of gaseous products. Finally, the flow returns to the tank and completes the loop. Any residual gases discharged to the tank escape the system through the ventilation system at the top of the tank. The plumbing of the loop exterior to the test section is based on 0.05-m nominal PVC, schedule 40 pipes and fittings. Figure 4 shows an upper portion of the test facility, including the top view of the superconducting magnet, the MHD and cryogenic plumbing, the video camera, and the mirror reflecting the top of the thruster.

B. Test Section

The helical thruster utilizes the cylindrical geometry of a solenoid magnet instead of the more conventional Cartesian geometry used with a dipole magnet. In this design, a radial electric current combined with an axial magnetic field creates an azimuthal Lorentz force and the subsequent flow. Components internal to the test section and the outer electrode are shown in Fig. 2. The flow enters and exits the acrylic caps of the test section through 0.044-m i.d., clear acrylic pipes.

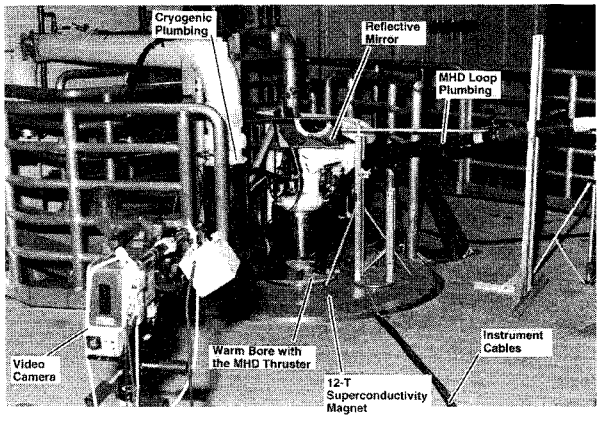

Fig. 4 Upper section of the MHD loop and the 12-T superconducting magnet.

The flow passage within each cap consists of a 90-deg elbow and a diffusion nozzle that is specially machined to provide a smooth transition between the circular flow area of the loop and the rectangular flow area of the MHD pumping region. The dimensions of the MHD pumping region are as follows: inner radius, 0.0704 m; outer radius, 0.116 m; electrode gap distance, 0.0455 m; electrode width, 0.0359 m; and helical fin pitch, 0.0406 m; which corresponds to a rise angle of 3.97 deg at the centerline of flow passage. Since the flow makes seven revolutions through the test section, the effective length of the thruster as defined by the arc length of the midline of flow passage is equal to 4.11 m, assuming seven conducting loops. The hydraulic diameter is 0.0401 m. Therefore, the AR based on electrode distance (L/D) is 90.3. If based on hydraulic diameter (L/D_h), it is 102.4.

The electrodes are insulated by PVC fins above and below the flow passage, allowing only seawater to conduct electricity in the MHD pumping region. The anode material is Hastelloy C-22 alloy and the cathode is DSE. DSE is a trade name for corrosion-resistant electrodes consisting of a titanium substrate coated with a rare-Earth (Ru or Ir) oxide thin film. The DSE coating for these experiments is iridium oxide. It should be stressed that the test section is originally designed to operate in a condition in which the magnetic field vector in the solenoid points downward. For these experiments, the superconducting solenoid has a fixed upward field, which causes the electrode polarity to be reversed from what is originally planned.

C. Magnet

The magnet used in the experiments is a 12-T superconducting solenoid magnet. It is 1.47 m in height with a 0.356-m-diam warm bore. This warm-bore dimension is significantly larger than the helical thruster. It suggests that there is plenty of room for improvement over the current helical device since the thruster performance increases with its size. The superconducting wires used are Nb_3Sn for the inner coils and NbTi for the outer pancake. They are all submerged in liquid helium under a subatmospheric pressure. It is important to point out that a subatmospheric pressure is necessary to maintain liquid helium at 1.8 K (instead of 4.2 K at 1 atm) for the maximum attainable current. Therefore, a large helium pump is required. The current required at 12 T is designed to be 2069 A. Because of its large size and surface area, the magnet has a large helium boil-off rate (50 l/h) due to heat leakage. For economic reasons, cryogenic helium recovery and liquefaction become necessary. The cost of this magnet is approximately $5–6,000,000 (see Ref. 16).

D. Instrumentation and Data Acquisition

The nature of the experiments is such that several physical parameters are monitored simultaneously (i.e., flow rate, electrode current, and voltage, etc.). To accomplish this a computer-aided data acquisition system is employed. All signals are conditioned such that 0–10-V analog signals are available to be used as inputs to a computer system.

The EG&G Flow Technology model FT-32 turbine flow meter with a model CAO-3 RF pickoff is used for these experiments. The RF pickoff operates by sensing a change of inductance due to the movement of a small magnet slug implanted in each blade of turbine. This operation is sensitive to an external magnetic field. Therefore, a magnetic shield of the flow meter is employed. A weight calibration of the flow meter is done prior to all experiments without a magnetic field. However, since the flow meter has been properly shielded in actual MHD tests, the magnetic field does not affect the flow meter performance.

The current to the electrodes is supplied by a Sorensen model DCR16-625T, SCR-regulated dc power supply. The supply is capable of providing 625 A at 16 V. The current output is remotely controlled by the data acquisition system.

A 300-A shunt resistor is used to measure the total current through the test section. The potential drop across the electrodes is measured at the test section. The temperature of solution is monitored using a resistance temperature detector (RTD) calibrated for the appropriate temperature range. As a backup, a J-type thermocouple is also employed. To measure the net pressure rise across the thruster, a Validyne model DP-15 differential pressure transducer is operated in conjunction with a Validyne model CD-23 digital transducer indicator. The conductivity of seawater is determined by the measured voltage–current relationship and the resistance formulations shown in Eqs. (4) and (5).

The data is collected using a Metrabyte model DAS-16F, high-speed A/D card with customized software. For a given field, the program sets the desired current and, after allowing the flow to stabilize, collects 1050 points of data per channel in approximately 30 s. At the end of the data collection, the mean and standard deviation of each parameter are calculated. Three data sets are collected at each of the current values. Once the data has been obtained for a given field, the magnetic field is changed and the process is repeated.

IV. Experiments Performed

Two different studies are performed to evaluate the performance of the helical thruster: 1) determination of hydraulic resistance of the loop and 2) the determination of the MHD-induced flow characteristics. The first experiments, hence referred to as calibration experiments, included measuring the hydraulic resistance of the test loop as a function of flow rate and electric current. This is done by placing a centrifugal pump in the test loop and measuring the pressure required to achieve a given flow rate at a given current and temperature. To conserve the allocated magnet time, these experiments are performed without a magnetic field. The current across the test section provides realistic bubble generation rates as would be seen in actual MHD tests. However, modification of the boundary-layer profile by MHD (or Hartmann) effect is not addressed by the calibration experiments. This data is placed in a data file. The gross pressure rise due to actual MHD pumping in the thruster can then be determined by interpolation within this file. This study also provides information about the combined frictional and form pressure drop across the thruster as a function of flow rate, current, and temperature. The K value in Eq. (6) can then be more realistically estimated based on the pressure drop information.

To determine the steady-state performance characteristics, a magnetic field strength is first established. At this point, a given electric current is applied to the electrodes that causes an MHD-induced flow. The flow is then allowed to stabilize. Once the flow has stabilized three data sets are taken. The data-acquisition software calculates the gross thrust, net thrust, and the corresponding efficiencies for each data set. In an actual MHD experiment, the net pressure rise across the thruster is physically measured. Therefore, the net thrust is easily determined. The gross thrust is obtained from the calibration data file mentioned previously as interpolated against the measured flow rate. The sequence is then repeated for each value of electric current at the same magnetic field strength. Once this has been completed, a new magnetic field setting is chosen and the procedure is repeated.

V. Results and Discussion

The analytical models described in Sec. II are used to predict the performance of the thruster. As mentioned in Sec. II.E., only the seven-conducting-loop configuration is modeled. In order to plot results vs current density, current density has been defined as current divided by an averaged electrode area, 1260 cm^2, between the inner and outer electrodes. Since this value is a constant, a given current will infer the same current density regardless of the number of conducting loops considered.

Figures 5–8 show both the theoretical and experimental flow rates, voltages, thrusts, and mechanical efficiencies at different current densities for the seven-conducting-loop system operating at 12 T. For results of other field strengths, see Ref. 17. Good agreement between theoretical and experimental results is achieved, especially with flow rate and voltage. As can be seen from Fig. 5, flow rate varies with current to a power of approximately one-half. This is expected because the MHD pressure rise varies linearly with applied current [Eq. (2)]. From Refs. 12 and 17, it can be seen that the hydraulic pressure should vary as the flow rate raised to a power slightly less than 2. Therefore, the flow rate should vary as the current (density) raised to a reciprocal of this

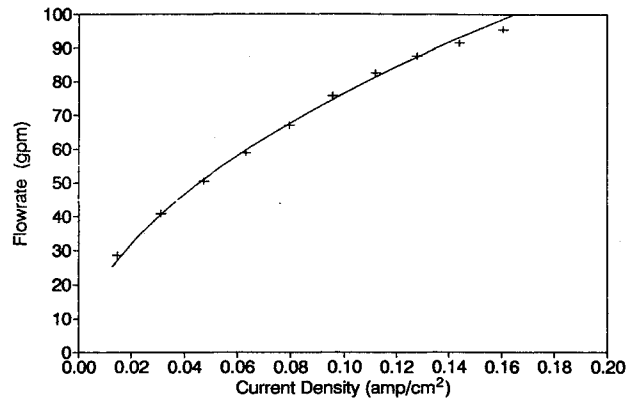

Fig. 5 Flow rate as a function of current density (B = 12 T). + = experiment and —— = theoretical.

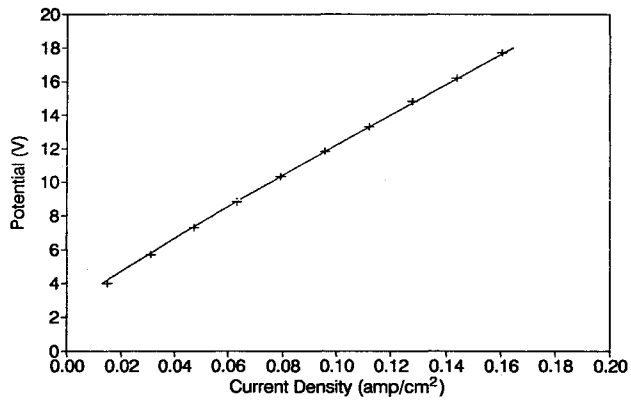

Fig. 6 Voltage as a function of current density (B = 12 T). + = experiment and —— = theoretical.

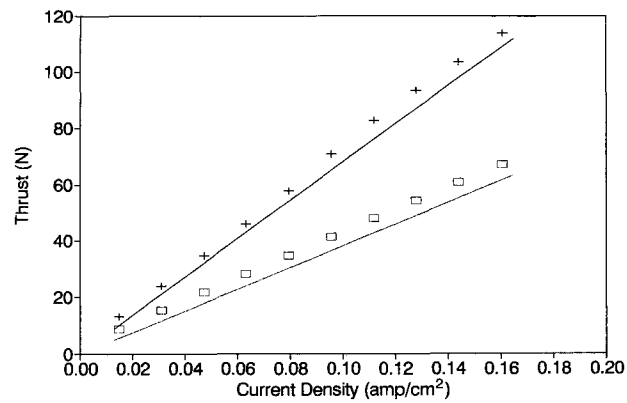

Fig. 7 Thrust as a function of current density (B = 12 T). + = gross (experiment), —— = gross (theory), □ = net (experiment), and ····· = net (theory).

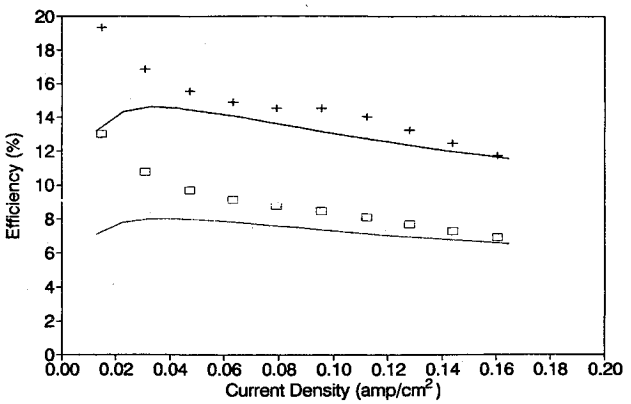

Fig. 8 Efficiency as a function of current density (B = 12 T). + = gross (experiment), —— = gross (theory), □ = net (experiment), and ····· = net (theory).

power. From the flow rate and cross-sectional area of the helical channel, it can be estimated that the fluid speed is as high as 3.7 m/s, as compared to 2.5 m/s when the same thruster is subject to a lower-field magnet (6–8 T).[12]

The voltage-current relationship is shown in Fig. 6. As predicted by Ohm's law, which describes the linear electrical behavior of a resistor, this is also a linear relationship with the exception of an overpotential offset. The extension of the experimental points near zero current density reveals that the electrolytic overpotential is about 2.41 V. The slope of the best-fit theoretical line suggests that, from Eq. (5), the seawater conductivity is about 4.84 $(\Omega m)^{-1}$, consistent with the conductivity meter readings. This information is then used by the theoretical model to calculate thrusts and efficiencies. When examining other voltage–current graphs at different magnetic fields,[17] it is interesting to note that the slope of the voltage–current line increases with increasing magnetic field. This is expected because at the same current, the required back EMF is larger for higher flow rate at a larger magnetic field.

Figure 7 shows the gross and net thrusts for both the experimental values and the theoretical prediction. The theoretical thrusts portray the same linear behavior, but consistently underpredict the experimental values. As discussed in Sec. II, the thrust varies linearly with electric current. The difference in magnitude between theory and experiment can be attributed to temperature and viscosity drifts during each experiment. The theoretical model predicts the gross thrust based on the flow rate measured and by finding out the pressure head required to generate such a flow rate from the calibration data file. Fluid temperature increases as the MHD test progresses. The flow meter then infers a higher flow rate than what it used to infer at room temperature for the calibration experiments, due to the decrease of viscosity. Consequently, the experimentally determined thrust is slightly higher than its theoretical counterpart. Additionally, the calibration experiments have not accounted for the boundary-layer modification by MHD (or Hartmann) effect. The discrepancy in net thrusts may be attributed to the drift of the pressure transducer calibration before and during the MHD thruster experiments. It is noted that the net thrust is approximately two-thirds of the gross thrust.

The plot of gross and net mechanical efficiencies (Fig. 8) shows that the theoretical models reasonably predict the behavior of the thruster. At high current densities, the efficiency varies as the current density raised to a power $\approx -\frac{1}{2}$. This effect can be seen from Eq. (9). Using the arguments from the flow rate discussion, the numerator will vary as $I^{1.5}$, whereas, if the applied voltage is large compared to the overpotential, the denominator will vary as I^2. At small currents, where the applied voltage is comparable to overpotential, the efficiency approaches to zero as the current is reduced to zero and the voltage to overpotential. This is illustrated by a condition where the current density is 0.01 A/cm² and a voltage of 3.8 V is required. Since the overpotential for the system is 2.41 V, only 1.4 V of the voltage applied is used to generate current. This causes a decrease in efficiency at lower voltages [Eq. (9)]. At low current density or low load factor, because the fluid velocity is low, the thruster pressure loss is very small since it scales with the square of velocity. As the current is increased, the overpotential effect diminishes and the efficiency begins to increase. This effect when combined with the trend of decreasing efficiency with increased current at high current density causes a peak efficiency to occur at approximately 0.03 A/cm².

This efficiency peaking is reflected by the theoretical curves, but not by the experimental data. The underpredictions of the theory are due to the same reasons discussed earlier for thrust (Fig. 7). Thrust is underpredicted for the entire range, therefore, so is efficiency. The larger underprediction at low current densities is primarily attributed to a propagation of experimental and theoretical errors. As can be seen from Eq. (9), the denominator becomes very small as both current and voltage decrease simultaneously, thus allowing small differences between theoretical and experimental potentials, thrusts, and velocities to be amplified in the calculation of efficiencies.

The gross efficiency of the helical thruster has scaled well with the magnetic field strength by comparing results of the previous 8-T and current 12-T experiments. As can be seen from Eq. (9), if I is maintained as a constant while the magnetic field strength varies, the numerator will increase with B^n, where n is approximately 1.5. It is because T scales linearly with B, and U scales with B raised to a power slightly greater than $\frac{1}{2}$ due to the Reynolds number dependence of the frictional factor. In the denominator V increases only mildly with B due to the back EMF. Thus, the gross efficiency scales with B raised to a power of approximately 1.5. This relationship has been verified by comparing the data from Fig. 8 and the previous 8-T data.[12] It has also been found that such a scaling relationship for a helical thruster is similar to that of a linear thruster, except significantly higher magnetic fields and a wider field range are available to the helical thruster.

Due to the electrode reversal, chemical attack of the Hastelloy-C shell by the anodic electrolytic reaction is observed. In addition to the warming of fluid by Joule heating, the chemical contamination of the solution may have contributed the uncertainty of the experiments that is reflected by the discrepancies in Figs. 7 and 8.

VI. Conclusions

Taking advantage of the 12-T superconducting solenoid magnet, the performance has been markedly improved for the same helical thruster at low fields (6–8 T).[12] The results of theoretical models are compared to the experimentally determined performance characteristics (flow rate, thrusts, and efficiencies). In both shape and magnitude, the predicted and experimental values are in good agreement. Many of the discrepancies are artifacts of the closed-loop environment. This leads to a change in the saltwater solution properties as the experiments progress. As discussed earlier, the reasons of performance improvement from a linear to a helical thruster are 1) significantly higher magnetic fields are available to helical thrusters with solenoid magnets, 2) large thruster AR (L/D) for MHD pumping in helical thrusters, 3) minimized fringe current loss due to the full circumferential coverage of the electrodes, and 4) reduced electric current density from a linear to a helical thruster using the same solenoid magnet, which significantly reduces the Joule heating. The efficiency achieved in this study is encouraging compared to many other linear thruster studies and our previous studies. All the dipole

magnets for linear thrusters used so far produce fields at 6 T or less, because it is very difficult to build a 12-T superconducting dipole, although theoretically a linear thruster (using a 12-T dipole) may be slightly more efficient than a helical thruster using a 12-T solenoid. In addition, the weight penalty paid by a dipole will always be higher on the basis of the same magnetic field strength and same warm bore size. With this 12-T superconducting solenoid, improved performance in both flow rate and efficiency are expected using a larger and more optimally designed helical thruster. More importantly, to prevent the artifact created by the closed-loop condition and to test with real ocean water that contains bio-organisms, open ocean thruster tests are essential.

In this set of experiments, in addition to gross thrust and efficiency, net thrust and efficiency are measured, computed, and compared. The net thrust and efficiency are more practical parameters of the thruster. For the particular helical thruster used, the net thrust is slightly less than two-thirds of the gross thrust. Future improvement of the thruster design will be focused at the reduction of internal losses, which tend to be more significant for helical thrusters than for linear thrusters.

Acknowledgments

The authors acknowledge the sponsorship of Office of Naval Research for this work, with G. D. Roy as the Scientific Officer of Grant N00014-89-J-1693. The Applied Research Laboratory of Pennsylvania State University provided additional financial support. Part of this work is done at Francis Bitter National Magnet Laboratory at the Massachusetts Institute of Technology, which is supported by the National Science Foundation. The support of L. G. Rubin, R. C. Johnson, R. L. Hans, and M. J. Coslo are also acknowledged.

References

[1]Lin, T. F., "Superconducting Magnetohydrodynamic Ship Propulsion—A Worldwide Research Effort," *Scientific Information Bulletin—Office of Naval Research Asian Office*, NAVSO P-3580, Vol. 17, No. 3, 1992, pp. 237–242.

[2]Motora, S., Imaichi, K., Nakato, M., and Takezawa, S., "An Outline of the Superconducting MHD Ship Propulsion in Japan," *Proceedings of the MHDS91 International Symposium on Superconducting Magnetohydrodynamic Ship Propulsion*, Japan Ship and Ocean Foundation, Kobe, Japan, 1991, pp. 53–68.

[3]Petrick, M., Thomas, A., Genens, L., Libera, J., Nietert, R., Bouillard, E., Hill, D., Picologolou, B., Ohlsson, O., Kasprzyk, T., and Berry, G., "Magnetohydrodynamic Seawater Propulsion," *Proceedings of the MHDS91 International Symposium on Superconducting Magnetohydrodynamic Ship Propulsion*, Japan Ship and Ocean Foundation, Kobe, Japan, 1991, pp. 175–187.

[4]Meng, J. C. S., Hrubes, J. D., Hendricks, P. J., Thivierge, C., and Henoch, C., "Experimental Studies of Superconducting Electromagnetic Thruster for Seawater Propulsion and Future Technology Challenges," *Proceedings of the MHDS91 International Symposium on Superconducting Magnetohydrodynamic Ship Propulsion*, 1991, pp. 203–210.

[5]Lin, T. F., Aumiller, D. L., Gilbert, J. B., Coslo, M. J., Brandt, B. L., and Rubin, L. G., "Study of the Influence of Electric and Magnetic Fields on Seawater Magnetohydrodynamic Propulsion," *Proceedings of the 2nd International Offshore and Polar Engineering Conference*, Vol. III, 1992, pp. 8–13.

[6]Doss, E., and Roy, G. D., "Flow Characteristics Inside MHD Seawater Thrusters," *Journal of Propulsion and Power*, Vol. 7, No. 4, 1991, pp. 635–641.

[7]Lin, T. F., Gilbert, J. B., and Roy, G. D., "Analyses of Magnetohydrodynamic Propulsion with Seawater for Underwater Vehicles," *Journal of Propulsion and Power*, Vol. 7, No. 6, 1991, pp. 1081–1083.

[8]Lin, T. F., "Consideration of Seawater Conductivity Enhancements for Electromagnetic Thrusters," *Proceedings of the 25th Inter-Society Energy Conversion Engineering Conference*, Vol. 5, 1990, pp. 552–556.

[9]Gilbert, J. B., Lin, T. F., Imblum, T. M., Naggar, J. A., Marks, S. P., and Bausch, M., "Seawater Conductivity Enhancement by Acid Seeding for Magnetohydrodynamic Propulsion," AIAA Paper 91-2499, June 1991.

[10]Lin, T. F., Marks, S. P., and Gilbert, J. B., "Seawater Conductivity Enhancement by Acid Seeding and the Associated Two-Phase Phenomena," *Proceedings of the MHDS91 International Symposium on Superconducting Magnetohydrodynamic Ship Propulsion*, Japan Ship and Ocean Foundation, Kobe, Japan, 1991, pp. 367–374 (Paper 11-3).

[11]Lin, T. F., Aumiller, D. L., Gilbert, J. B., and Coslo, M. J., "Analytical and Experimental Studies of the Cyclic Magnetohydrodynamic Thruster Designs," *International Journal Offshore and Polar Engineering*, Vol. 3, No. 4, 1993, pp. 250–257.

[12]Gilbert, J. B., Aumiller, D. L., and Lin, T. F., "Analytical and Experimental Studies of the Helical Magnetohydrodynamic Thruster Design," Pennsylvania State Univ., Applied Research Lab. TM 93-079, University Park, PA, 1993, pp. 1–38.

[13]*Flow of Fluids Through Valves, Fittings and Pipe—(Metric Edition)*, Crane Co., Technical Paper 410M, King of Prussia, PA, 1986.

[14]Incropera, F. P., and Dewitt, D. P., *Fundamentals of Heat and Mass Transfer*, Wiley, New York, 1986, pp. 372–374.

[15]Whitfield, M., and Jagner, D. (ed.), *Marine Electrochemistry: A Practical Introduction*, Wiley-Interscience, New York, 1981, p. 507.

[16]Iwasa, Y., Leupold, R. J., Weggel, R. J., Williams, J. E. C., and Itoh, S., "Hybrid III: The System, Test Results, the Next Step," *IEEE Transactions on Applied Superconductivity*, Vol. 3, 1993, pp. 58–62.

[17]Lin, T. F., Gilbert, J. B., Johnson, R. C., Hans, R. L., and Coslo, M. J., "Studies of a Helical MHD Thruster in a 12-Tesla Superconducting Solenoid Magnet," Pennsylvania State Univ., Applied Research Lab. TM 93-137, University Park, PA, 1993, pp. 1–28.